ACS OMEGA

Open Access

http://pubs.acs.org/journal/acsodf

Article

Exploring Metal Nanocluster Catalysts for Ammonia Synthesis Using Informatics Methods: A Concerted Effort of Bayesian Optimization, Swarm Intelligence, and First-Principles Computation

Yuta Tsuji,* Yuta Yoshioka, Kazuki Okazawa, and Kazunari Yoshizawa

Cite This: *ACS Omega* 2023, 8, 30335−30348

Read Online

ACCESS | Metrics & More | Article Recommendations | Supporting Information

ABSTRACT: This paper details the use of computational and informatics methods to design metal nanocluster catalysts for efficient ammonia synthesis. Three main problems are tackled: defining a measure of catalytic activity, choosing the best candidate from a large number of possibilities, and identifying the thermodynamically stable cluster catalyst structure. First-principles calculations, Bayesian optimization, and particle swarm optimization are used to obtain a Ti_8 nanocluster as a catalyst candidate. The N_2 adsorption structure on Ti_8 indicates substantial activation of the N_2 molecule, while the NH_3 adsorption structure suggests that NH_3 is likely to undergo easy desorption. The study also reveals several cluster catalyst candidates that break the general trade-off that surfaces that strongly adsorb reactants also strongly adsorb products.

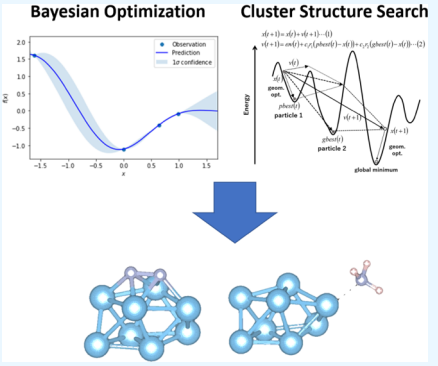

1. INTRODUCTION

The Haber−Bosch process[1] is used in industrial ammonia synthesis. In this process, ammonia is synthesized from nitrogen and hydrogen molecules as follows

$$\frac{1}{2}N_2 + \frac{3}{2}H_2 \rightleftarrows NH_3 \quad (1)$$

Ammonia synthesized has diverse applications, including its use as a nitrogen fertilizer, in the production of explosives, as refrigerants, and as materials for energy storage. The uses of the synthesized ammonia are diverse, including nitrogen fertilizer, explosive production, refrigerants, and energy storage materials.[2] Among the many uses for ammonia, nitrogen fertilizer accounts for a very large proportion, and this method supports a food supply that feeds about half of the world's population.[3]

The reaction Gibbs free energy change for the reaction in eq 1 is −32.37 kJ/mol at 300 K.[4] However, the reaction barrier is extremely high, so without a catalyst, the nitrogen−hydrogen mixture would not produce ammonia to any appreciable degree. In the Haber−Bosch process, the catalyst is active α-Fe, which is made by reducing Fe_3O_4 mixed with K_2O, an electronic promoter that improves catalytic activity, and SiO_2 and Al_2O_3, structural promoters that stabilize the catalyst structure.[5] In the equilibrium reaction shown in eq 1, the formation of ammonia is favored in a low-temperature, high-pressure environment. However, a high-temperature environment is necessary to increase the reaction rate. The Haber−Bosch process is usually operated at 400−500 °C and 10^2−10^3 atm in the presence of the catalyst.[6]

As mentioned above, the implementation of the Haber−Bosch process requires high-temperature and high-pressure conditions, which is a high energy-consuming process, emitting very large amounts of CO_2 and placing a significant burden on the natural environment. It is said that ammonia synthesis plants emit CO_2 equivalent to 1.44% of the world's CO_2 emissions.[7] Therefore, most of the recent research is aimed at realizing a more environmentally friendly and economical method than the Haber−Bosch process. There are many examples of homogeneous catalysts that mimic the mechanism of catalytic conversion of nitrogen by a metalloenzyme called nitrogenase.[8,9] Heterogeneous catalytic ammonia synthesis using metal nanoparticles supported on electride surfaces[10−12] and hydrides of early transition metals such as Ti and V[13−15] has also been studied extensively. In addition, various materials such as nitrides,[16,17] alloys,[18,19] and intermetallic compounds[20,21] are being considered as potential catalysts for ammonia synthesis. Since we cannot review here all of the efforts of many researchers in creating innovative heterogeneous catalysts for ammonia synthesis, we refer the reader to some review articles[22−24] for more details.

Received: May 17, 2023
Accepted: July 21, 2023
Published: August 7, 2023

Many of the heterogeneous catalysts cited above are characterized by metal nanoparticles supported on inorganic material surfaces. Recently, catalytic reactions by metal nanoclusters and metal sub-nanoclusters, which are even smaller groups of metal atoms than metal nanoparticles, have attracted much attention.[25,26] Metal clusters exhibit unique properties beyond those expected from bulk metals, and the reactivity of metal clusters changes discontinuously when the number of constituent atoms is changed one by one.[27,28] Such reactivity is attributed to the fundamental physical properties of clusters, including their overall shape, geometric structure, electronic structure, and thermodynamic properties.[29,30] In particular, clusters have a larger proportion of surface area than nanoparticles, and the increase in the number of sites with coordination unsaturation, such as edges and corners, is thought to be one reason why chemical reactions occurring on the cluster surface are efficient.[31−33]

So far, we have reviewed what is generally known about cluster catalysts. Now we will look at how clusters can be of benefit to ammonia synthesis specifically. Li et al.[34] synthesized Ru catalysts ranging in size from atomic clusters and subnanometer clusters to nanoparticles, and found that Ru atomic clusters exhibit a very high turnover frequency (TOF) in ammonia synthesis. As the size of Ru decreases to the nanolevel, the number of B5 and terrace sites decreases, and the N_2 activation pathway changes; the reaction pathway for NH_3 synthesis is altered, thus improving catalytic performance. The enhanced intra-cluster interactions of Ru_3-atom clusters shift the d-band center of Ru and promote the adsorption and activation of N_2 on the catalyst, leading to the formation of NH_3 via a low activation barrier. Liu et al.[35] proposed the use of Fe_3 clusters supported on the θ-Al_2O_3 (010) surface as heterogeneous catalysts for ammonia synthesis: due to the large spin polarization of the Fe_3 cluster, the low oxidation state of iron, and its multistep redox capacity, the TOF of the Fe_3 catalyst was found to be comparable to that of the conventional Ru catalyst. Ma et al.[36] found that the bimetallic cluster of Rh_1Co_3 dispersed on the surface of CoO (011) exhibits high catalytic activity for ammonia synthesis due to the charge buffering ability of the doped low-valent metal Rh and the complementary role of the synergistic metal Co. Peng et al.[37] successfully synthesized a catalyst consisting of Co dimers dispersed on an N-doped carbon support. They found that electron-rich Co serves as an efficient site for promoting donation and back-donation behavior between Co and N_2 molecules during NH_3 synthesis, facilitating the activation of N_2 and its subsequent stepwise hydrogenation to NH_3.

As detailed above, metal nanoclusters can be found to combine a number of properties to facilitate ammonia synthesis. The properties will depend on the type of metal elements that make up the cluster, the number of metal atoms, and the support. Selecting the best catalyst from among these myriad candidates is a very difficult task. We would consider tackling this challenge with the help of informatics techniques that have been advancing in recent years. A field called catalytic informatics is emerging. Several review and concept articles have been written on this field.[38−41] Indeed, a wide variety of informatics methods are becoming available to aid in catalyst development.

Our goal in this study was set to search for suitable metal nanoclusters for ammonia synthesis. In many cases, catalytic informatics research is very compatible with computational methods such as first-principles calculations and is also combined with high-throughput calculations.[42−44] Therefore, we have combined first-principles calculations with informatics methods in this study to tackle the challenge of ammonia synthesis.

We focused on Bayesian optimization (BO)[45,46] to achieve the objectives of this study. BO is a powerful machine learning technique that can optimize a black box function with a limited number of evaluations.[47−49] In the context of nanocluster catalyst design, BO can be used to efficiently explore the vast space of possible combinations of the type and number of metal atoms constituting a nanocluster and to identify the optimal composition of nanoclusters that maximizes the desired catalytic properties.

The use of BO for the design of nanocluster catalysts has several advantages over conventional methods. For example, it can efficiently search for higher dimensional spaces of possible compositions. Traditional methods such as brute-force enumeration and random sampling quickly become computationally infeasible as the number of possible compositions increases.[50,51] BO, on the other hand, uses a stochastic model to perform the search,[52,53] which allows the space to be explored efficiently.

In recent years, many examples of the use of BO have been reported in a wide range of catalyst development and catalyst applications. Pedersen et al.[54] reported that they performed BO on a model based on density functional theory (DFT) to predict the most active high-entropy alloy composition for the electrochemical oxygen reduction reaction with as few sampling compositions as possible. Nugraha et al.[55] demonstrated that BO can efficiently aid in designing experiments to discover the optimal composition of metal precursors, yielding mesoporous ternary metal PtPdAu alloys with enhanced electrocatalytic activity in methanol oxidation. Nagai et al.[56] applied BO to the drying process of catalyst inks for polymer electrolyte fuel cells to determine optimal drying conditions with a small number of trials. Okazawa et al.[19] used a combination of BO and DFT calculations to find the optimal binary alloy catalyst for the nitrogen activation reaction.

The combined approach of DFT calculations and BO is becoming more common, not only in catalyst development, but also in various other areas of materials development.[47,57,58] However, to our knowledge, this approach has not been applied to the development of nanocluster catalysts. One of the reasons for this may be the structural diversity of the nanoclusters. Consider choosing the catalytic activity of a nanocluster as the objective function for BO and evaluating it with a DFT calculation. To perform a DFT calculation, one must first determine the structure of the nanocluster. Predicting the ground-state structure of a cluster corresponding to the global minimum of the potential energy surface is a difficult task. In general, the number of local minima increases exponentially with increasing cluster size.[59]

To address this problem, it is effective to utilize evolutionary algorithms, such as genetic algorithm (GA) and particle swarm optimization (PSO).[60−63] The comparison between PSO and GA in terms of cluster structure search has already been discussed in the literature,[64,65] but the main difference may be that GA has a selection process characterized by survival of the fittest, whereas PSO has no such process. PSO requires a relatively small population size and converges more quickly than GA.[65] That is why we focus on cluster structure search using PSO.

https://doi.org/10.1021/acsomega.3c03456
ACS Omega 2023, 8, 30335−30348

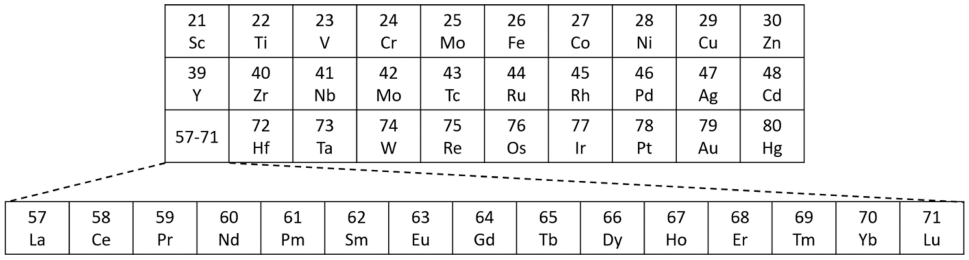

Figure 1. List of elements (part of the periodic table) constituting the metal nanoclusters targeted for exploration in this study.

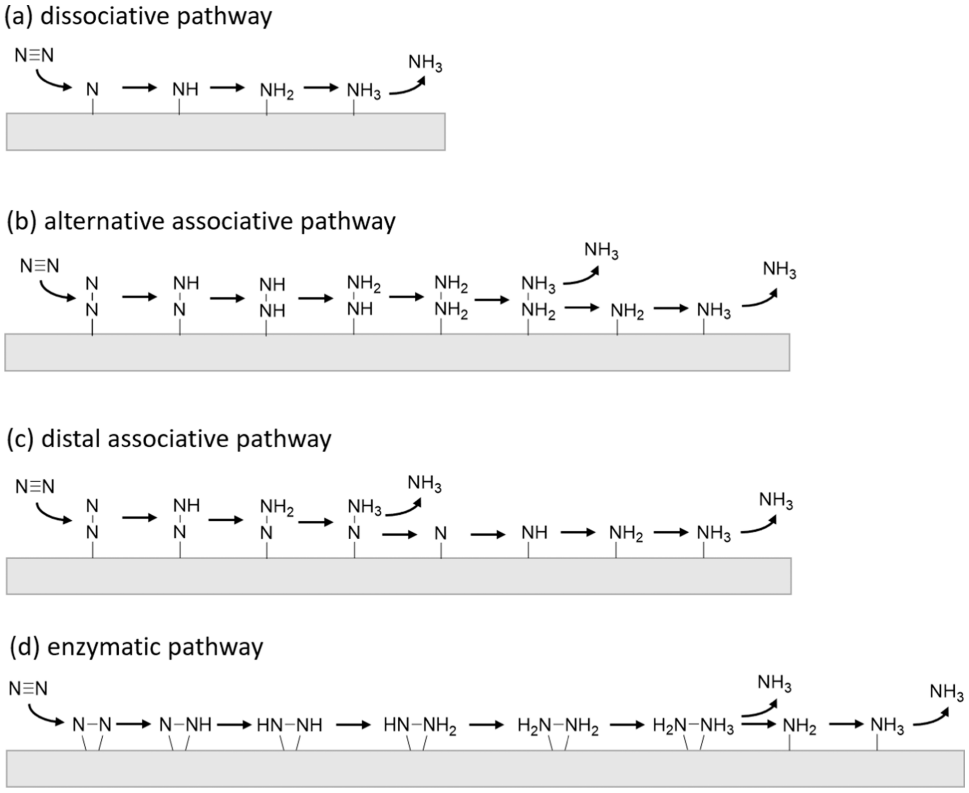

Figure 2. Schematic diagram of four typical ammonia synthesis pathways that are known to occur on solid surfaces: (a) dissociative, (b) alternative associative, (c) distal associative, and (d) enzymatic pathways.

The PSO algorithm was proposed by Kennedy and Eberhart in 1995, inspired by the social behavior of a flock of birds or fish.[66] In the context of predicting the structure of metal nanoclusters, PSO can be used to search for the most stable arrangement of atoms within a cluster. The objective function is usually defined as the total energy of the system, calculated using quantum mechanical methods such as DFT. We have been using the PSO algorithm to search for cluster structures.[67−69]

The purpose of this study is to attempt to explore metal nanocluster catalysts for ammonia synthesis by combining DFT calculations with two informatics tools, namely, BO and PSO. We will model the complex phenomenon of catalysis and theoretically challenge the development of catalysts with the support of informatics and computational chemistry. The evaluation of catalytic activity based on DFT calculations and the structure search combining DFT calculations and PSO algorithm are very computationally demanding tasks. By combining BO here, we have planned to improve the efficiency of our work. This paper describes our efforts to do so. The structure of this paper is as follows. We first address the problem clarification. We then consider how to model the problem and apply the tools of informatics and computational chemistry to it. Finally, we analyze the results.

2. RESULTS AND DISCUSSION

2.1. Clarification of Issues to Be Addressed. The properties of a metal nanocluster catalyst for ammonia synthesis are affected by the type and number of atoms that make up the cluster and the type of support. However, as it stands, the problem is too complex to be expected to be solved at all, so let us simplify the problem just a bit more. In this study, (1) we ignore the influence of the support, and (2) we assume that there is only one type of metal element that makes up the metal nanocluster.

Figure 1 shows the 44 elements targeted for exploration in this study. Based on our investigation of previous studies,[34−37] we defined the target of our search as a part of the periodic table dominated by transition metals. In previous studies,[34,35,37] clusters consisting of relatively few atoms such as Co_2, Ru_3, and Fe_3 have been thoroughly investigated. We have selected clusters consisting of four or more atoms as an

https://doi.org/10.1021/acsomega.3c03456
ACS Omega 2023, 8, 30335−30348

unexplored area worth exploring. Nevertheless, due to computational resource limitations, we set an upper limit of 10 atoms for the size of the clusters we explore. Based on the above, the size of our search space in this project consists of 308 nanocluster candidates.

2.2. Evaluation Method for Nanocluster Catalytic Activity. We intend to evaluate the catalytic activity for ammonia synthesis for the candidate metal nanocluster catalysts and use it as the objective function for BO. In this way, we will be able to efficiently extract a cluster with the optimal catalytic activity from the 308 metal nanocluster candidates discussed in the previous section. To do so, we must define what we mean by catalytic activity for ammonia synthesis. Catalytic activity is generally defined by the rate of reaction.[70,71] One idea to estimate the catalytic activity computationally would be to use the activation barrier of the rate-limiting step. If it is low, the reaction rate will be high, and the catalytic activity of such a catalyst will be high.

What is the rate-limiting step in ammonia synthesis? Figure 2 shows the generally accepted typical mechanisms of ammonia synthesis.[72−74] In the Haber−Bosch process with iron- or ruthenium-based catalysts, it is known that the reaction proceeds along the dissociative pathway, as shown in Figure 2a.[75−77] The rate-limiting step in this process is known as the dissociative chemisorption of N_2.[5,75,76,78] Since the computational cost of DFT calculations of transition states for estimating activation barriers is very high, it may be possible to use, for example, the reaction heat of dissociative adsorption of N_2 as an indicator of catalytic activity.[19] In such a study, Hammond's postulate[79] and the Bell−Evans−Polanyi principle[80,81] are assumed. If the reaction mechanism is limited to the dissociative pathway only, the search for catalysts can be based on the adsorption energy of nitrogen atoms; Nørksov and co-workers argue that this is the best descriptor.[82] In fact, the design of high-entropy alloy nanoparticles based on nitrogen adsorption energy has recently been reported.[83]

Previous studies have suggested that the mechanism of cluster-catalyzed ammonia synthesis is more complex. In most cases, ammonia synthesis on cluster catalysts proceeds by an associative mechanism.[34−36] That is why it does not seem possible to use the dissociative adsorption energy of N_2 as an indicator of catalytic activity in the search for the optimal cluster catalyst.

As such, we decided to focus on one elementary process common to all pathways. It is the physisorption of N_2. In fact, the sticking coefficient (probability) of N_2 on the surface of iron catalysts in the Haber−Bosch process is known to be very small, around 10^{-6},[84,85] and the ease of N_2 adsorption on the catalyst surface is likely to affect the reaction rate. Surface science measurements by Ertl et al.[86] showed that the addition of potassium to Fe catalysts increased the magnitude of the adsorption energy of molecular nitrogen and enhanced the dissociation of nitrogen molecules.

In light of the above, and considering that the first step in any ammonia synthesis process is the adsorption of N_2, without which nothing will happen, using the adsorption energy of N_2 as an indicator of catalytic activity is still not a bad choice. The adsorption energy of N_2 (E_{ads}) is defined by the following equation:

$$E_{ads} = E_{N_2/cluster} - (E_{N_2} + E_{cluster}) \quad (2)$$

where $E_{N_2/cluster}$ means the energy of a complex system with an N_2 molecule adsorbed on a cluster, E_{N_2} means the energy of the N_2 molecule alone, and $E_{cluster}$ means the energy of the cluster alone.

Figure 3 shows two typical adsorption modes of N_2 on metal nanocluster surfaces.[87,88] If the side-on adsorption mode is more stable than that of the end-on mode, it is assumed that N_2 adsorbed in the end-on mode would transition to the side-on mode during the geometry optimization process. Therefore, we used the end-on type adsorption structure as the initial structure for the geometry optimization of the adsorption structure for the calculation of the adsorption energy of N_2 onto the nanoclusters. Geometry optimization was performed using the end-on adsorption structure on all symmetrically distinct metal atoms in the nanoclusters as the initial structure. Thus, multiple values of E_{ads} may be obtained for a single metal nanocluster, in which case, the value with the largest magnitude of E_{ads} was adopted. For details on setting up geometry optimization calculations, refer to Section 4 at the end of this paper.

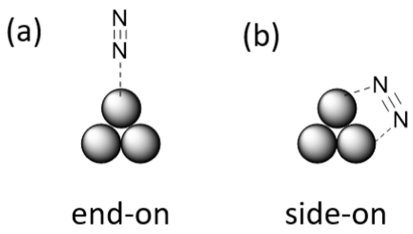

Figure 3. Two typical adsorption modes of N_2 on metal nanocluster surfaces: (a) end-on and (b) side-on.

Here, we should not forget what Sabatier's principle[89] tells us. So far, Sabatier's principle has provided a conceptual framework for the search for the optimal catalyst in catalyst development. If the interaction between the catalyst and molecule is too weak, the molecule cannot bind to the catalyst, and the reaction will not occur. On the other hand, if the interaction is too strong, the product will not be desorbed. In other words, the optimal catalyst condition is to bind molecules with an intermediate strength. That is why plotting the reaction rate as a function of the strength of the interaction between the molecule and the catalyst surface yields the so-called volcano plot shown in Figure 4. Such a concept, of course, also applies to ammonia synthesis.[90,91]

In light of the above, it would be unwise to rely solely on the adsorption energy of the N_2 molecule to search for an optimal catalyst. This is because the catalyst may be poisoned and inactivated. Therefore, the ease of product desorption, i.e., the NH_3 desorption barrier, should also be taken into account.[92] We need to introduce a term in the objective function that relates to the acceleration of product desorption. The barrier to desorption of NH_3 from metal nanoclusters (E_{des}) is calculated by the following equation:

$$E_{des} = E_{NH_3} + E_{cluster} - E_{NH_3/cluster} \quad (3)$$

where $E_{NH_3/cluster}$ means the energy of a complex system with an NH_3 molecule adsorbed on a cluster and E_{NH_3} means the energy of the NH_3 molecule alone. As adsorption sites for NH_3 to calculate $E_{NH_3/cluster}$, on-top type adsorption modes at all symmetrically unique metal atom positions were considered, as

https://doi.org/10.1021/acsomega.3c03456
ACS Omega 2023, 8, 30335−30348

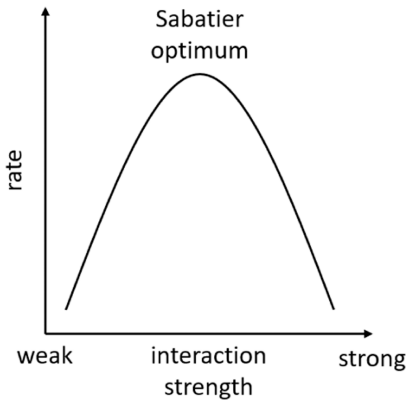

Figure 4. Schematic diagram qualitatively representing the Sabatier principle. This is what is called a volcano plot.

in the calculation of N_2 adsorption. In other words, an adsorption structure was assumed in which a lone pair on the N atom of NH_3 coordinates on a single metal atom in the cluster.

In general, when N_2 is adsorbed, the energy of the system goes down, so $E_{ads} < 0$. On the other hand, when NH_3 is desorbed, the energy of the system goes up, so $E_{des} > 0$. To achieve Sabatier optimal, E_{ads} should be more negative. That is, the absolute value of E_{ads} should be as large as possible. On the other hand, E_{des} should be as small as possible and close to 0. In other words, its absolute value should be as small as possible. In light of the above, we define $y = |E_{ads}| - |E_{des}|$ as a measure of catalytic activity. The larger the value of y, the higher the catalytic activity is expected. In this study, we utilize BO to find metal nanoclusters in which the value of y is as large as possible. In other words, we set y as the objective function for BO.

2.3. Determination of Initial Data Set Size in Preparation for BO Execution. In this study, BO was performed using PHYSBO (optimization tool for PHYSics based on Bayesian Optimization),[93,94] a Python library for fast and scalable BO. It is an enhanced version of COMBO[95] for materials science. Recently, many examples of BO applications in the field of materials science using PHYSBO have been reported.[19,96−99]

The space to be explored by BO is prepared in advance. That is, the explanatory variables for the candidate materials are represented by a vector $\mathbf{x}$ and listed. At this stage, the value of the objective function is not known. Among these, a few candidates are selected for the construction of the initial data set, and the value y of the objective function is estimated by DFT calculations. This yields the training data $D = \{\mathbf{x}_i, y_i\}_{(i = 1,\cdots,N)}$, where N represents the number of initial data points. To perform BO, at least two or more objective function values must be obtained.[100] The number of initial data points required depends on the problem to be optimized, the size of the search space, etc.[100]

In this study, we set $N = 5$. As discussed in Section 2.1, our search space consists of 308 candidate nanoclusters. Therefore, the proportion of the initial data set to the total number of data samples is 5 out of 308 (approximately 1.6%). Compare this ratio with previous studies: the ratio of initial data sets in the BO-based screening by Seko et al. is 0.2%[58] and that by Hashimoto et al. is 0.4%.[47] In light of the above, we can say that the initial data set size of $N = 5$ is a large enough size.

2.4. Selection of Explanatory Variables. BO can only begin after the candidate compounds have been encoded with an appropriate set of feature vectors (explanatory variables). In BO, the selection of appropriate feature vectors is the most important and often the most difficult part, so considerable research activity is devoted to the development of feature vectors.[101−103] The feature vector $\mathbf{x}_i$ for the i-th candidate is written down as follows:

$$\mathbf{x}_i = (x_1^{(i)}, x_2^{(i)}, \cdots, x_n^{(i)}) \tag{4}$$

where n is the dimension of vector $\mathbf{x}_i$, i.e., the number of explanatory variables. We assume that the value of the objective function for the i-th substance, i.e., y_i, is expressed as a function of $\mathbf{x}_i$

$$y_i = f(\mathbf{x}_i) = f(x_1^{(i)}, x_2^{(i)}, \cdots, x_n^{(i)}) \tag{5}$$

Thus, of course, the elements of $\mathbf{x}_i$ should have a meaningful relationship to y_i. However, it is very difficult to find such variables. Moreover, such variables need to be quite easily measurable compared to the objective variable. Otherwise, there is no need to bother with BO.

Higher dimensioning of $\mathbf{x}_i$ may be one way to address such an issue. A wide variety of features such as ionization energy, electronegativity, electron affinity, number of valence electrons, and atomic size have been used in machine learning studies for the design of various inorganic materials, including perovskites[104] and high-entropy alloys.[105] However, such an approach should not be taken too easily in BO implementation. This is because the inclusion of many variables through higher dimensioning of $\mathbf{x}_i$ might badly affect the assessment of similarity between candidate materials,[101] which is calculated from the distances between feature vectors for different candidate materials and plays a crucial role during the calculation of the posterior distribution. It is reported that BO using high dimensional feature vectors often performs very poorly.[101] As such, in order to efficiently perform BO, it is first necessary to identify a minimum set of features related to the material properties of interest and to construct a low-dimensional feature vector. That is why we decided to consider the type of metal atom and cluster size as the minimum required feature vector elements to dictate the composition of metal nanoclusters in this study. The type of metal atom is specified by its atomic number, and the cluster size is specified by the number of atoms in the cluster.

2.5. Preparation and Analysis of the Initial Data Set for BO. We need to calculate E_{ads} for N_2 adsorption and E_{des} for NH_3 desorption for five metal nanoclusters and determine the value of the objective function y. To do this, we need to determine the structure of the five metal nanoclusters. We do this using a combination of DFT calculations and the PSO algorithm. This is a very costly calculation. We thought we would save a little bit of computational resources. We had already determined the structures of the Fe_5, Ni_5, and Cu_5 clusters in our previous work.[69] So, we used those structures to evaluate E_{ads} and E_{des}. We determined that the number of metal nanoclusters comprising the initial data set was 5, so we needed 2 more. We randomly selected Sc_8 and Ce_9.

Table 1 lists the E_{ads}, E_{des}, and $y = |E_{ads}| - |E_{des}|$ values calculated for the clusters selected above. The index of catalytic activity, y, spans a wide range from −0.40 to 2.57 eV, suggesting that proper sampling has been achieved. Based on

https://doi.org/10.1021/acsomega.3c03456
ACS Omega 2023, 8, 30335−30348

Table 1. List of E_{ads} and E_{des} Values Calculated for Each Cluster Comprising the Initial Data and the Index of Catalytic Activity $y = |E_{ads}| - |E_{des}|$ Calculated from Them[a]

	E_{ads} (eV)	E_{des} (eV)	$y = \lvert E_{ads}\rvert - \lvert E_{des}\rvert$ (eV)
Fe_5	−0.98	0.24	0.74
Ni_5	−1.47	1.32	0.15
Cu_5	−0.59	1.00	−0.40
Sc_8	−3.40	0.84	2.57
Ce_9	−2.94	0.83	2.11

[a]All numbers are rounded to two decimal places. y was calculated on the data before rounding, and the result is rounded to two decimal places.

the initial data, Sc_8 is the best nanocluster catalyst candidate that meets our requirements for the catalyst.

It would be instructive to look for differences in structure between those with the highest and lowest y values in Table 1. Figure 5 shows the structures obtained by geometry

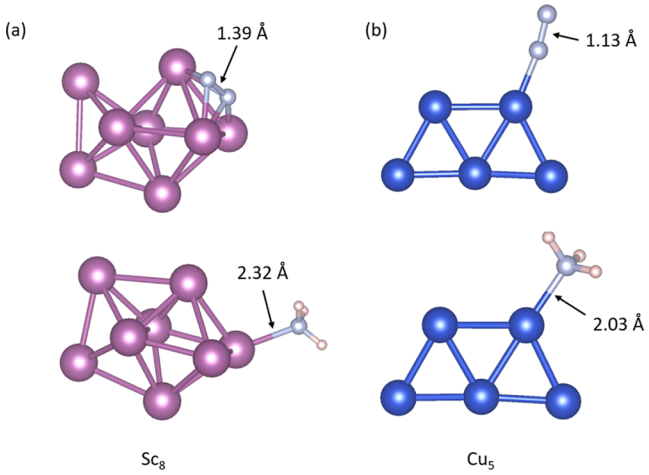

Figure 5. Optimized adsorption structures of N_2 and NH_3 on (a) Sc_8 and (b) Cu_5. Selected bond distances are shown.

optimization of N_2 and NH_3 adsorbed on Sc_8 and Cu_5. The Sc_8 cluster, optimized using the PSO algorithm, has an adjacent bicapped octahedron structure; the Cu_5 cluster has a planar trapezoidal two-dimensional structure. The most stable structures of these metal clusters have been reported in previous studies.[106−108] The structures of these clusters that we have identified using PSO are in perfect agreement with those reported in the previous studies. Ideally, one would like to compare the computationally determined structures with experimental results, as has been done in recent studies,[109,110] but a comparison with the structures presented in the literature provides some evidence that the PSO algorithm is good at accurately searching for stable structures. On Sc_8, N_2 is adsorbed in the side-on mode, while on Cu_5 it is adsorbed in the end-on mode. In both cases, N_2 was set to the end-on adsorption mode in the initial structure of the optimization, but during the optimization process, a transition from the end-on to the side-on mode occurred in the case of Sc_8. The N−N bond length of N_2 adsorbed on Sc_8 is 1.39 Å, whereas that on Cu_5 is 1.13 Å. The N−N bond length is an indicator of nitrogen activation,[13] suggesting that N_2 on Sc_8 is more activated than that on Cu_5. On the other hand, the bond distance between the metal atom and the N atom in the NH_3 adsorption structure would be considered an indicator of the desorption barrier: on Sc_8, the distance between the Sc atom and NH_3 is 2.32 Å, while on Cu_5, it is 2.03 Å. Thus, it is expected that Sc_8 is more likely to release NH_3. From these observations, we may conclude that our definition of y is a good indicator for conveniently estimating catalytic activity. Note, however, that this is only a formulation of the necessary conditions that a catalyst must satisfy, not a sufficient condition. Other indicators may be useful if one wants to search for catalysts only for a particular reaction mechanism (e.g., dissociative pathway). In this study, our research is designed with the intention of optimizing cluster catalysts with diverse catalytic reaction pathways at the lowest possible computational cost.

2.6. Learning Initial Data Using Gaussian Processes. A Gaussian process regression (GPR) is performed using y in Table 1 and the atomic number of the metal atom and the number of metal atoms in each metal cluster, $\mathbf{x}$. The GPR prediction of catalytic activity, $\mu(\mathbf{x})$, and the variance, $\sigma(\mathbf{x})$, associated with the uncertainty of the prediction are calculated according to the following equations:[95,100]

$$\mu(\mathbf{x}) = \mathbf{k}(\mathbf{x})^{\mathrm{T}}(\mathbf{K} + \lambda\mathbf{I})^{-1}\mathbf{y} \tag{6}$$

and

$$\sigma(\mathbf{x}) = k(\mathbf{x}, \mathbf{x}) + \lambda - \mathbf{k}(\mathbf{x})^{\mathrm{T}}(\mathbf{K} + \lambda\mathbf{I})^{-1}\mathbf{k}(\mathbf{x}) \tag{7}$$

where $\mathbf{I}$ is the unit matrix and k is a function called a kernel. GPR is a regression model that can express various functions by designing kernel functions. In GPR, the kernel function $k(\mathbf{x}_i, \mathbf{x}_j)$ can be used to express the similarity of two input data points $\mathbf{x}_i$ and $\mathbf{x}_j$, among a set of data points.[47] There are various kernels available, but the following Gaussian kernel, or radial basis function (RBF) kernel, is generally used[100]

$$k(\mathbf{x}_i, \mathbf{x}_j) = \exp\left(-\frac{1}{2\eta^2}\|\mathbf{x}_i - \mathbf{x}_j\|^2\right) \tag{8}$$

λ and η that appear in the above equations are called hyperparameters; PHYSBO has the ability to optimize these values. Using the RBF kernel, $\mathbf{k}(\mathbf{x})$ and $\mathbf{K}$ are calculated as follows

$$\mathbf{k}(\mathbf{x}) = [k(\mathbf{x}_1, \mathbf{x}), k(\mathbf{x}_2, \mathbf{x}), \cdots, k(\mathbf{x}_N, \mathbf{x})]^{\mathrm{T}} \tag{9}$$

and

$$\mathbf{K} = \begin{bmatrix} k(\mathbf{x}_1, \mathbf{x}_1) & k(\mathbf{x}_1, \mathbf{x}_2) & \cdots & k(\mathbf{x}_1, \mathbf{x}_N) \\ k(\mathbf{x}_2, \mathbf{x}_1) & k(\mathbf{x}_2, \mathbf{x}_2) & \cdots & k(\mathbf{x}_2, \mathbf{x}_N) \\ \vdots & \vdots & \ddots & \vdots \\ k(\mathbf{x}_N, \mathbf{x}_1) & k(\mathbf{x}_N, \mathbf{x}_2) & \cdots & k(\mathbf{x}_N, \mathbf{x}_N) \end{bmatrix} \tag{10}$$

N is the number of samples in the training data. In this study, $N = 5$. By applying eqs 6 and 7 to all candidate points for which y values have not yet been observed, we can estimate the predicted value of y and the uncertainty of the prediction at each candidate point. Based on the predictions and their uncertainties thus obtained, the value of the acquisition function (AF) at each candidate point is evaluated to determine the next observation point.

As an economical search method, it is important that the algorithm maintains a balance between exploring regions of high uncertainty and updating the optimal value by exploring

https://doi.org/10.1021/acsomega.3c03456
ACS Omega 2023, 8, 30335−30348

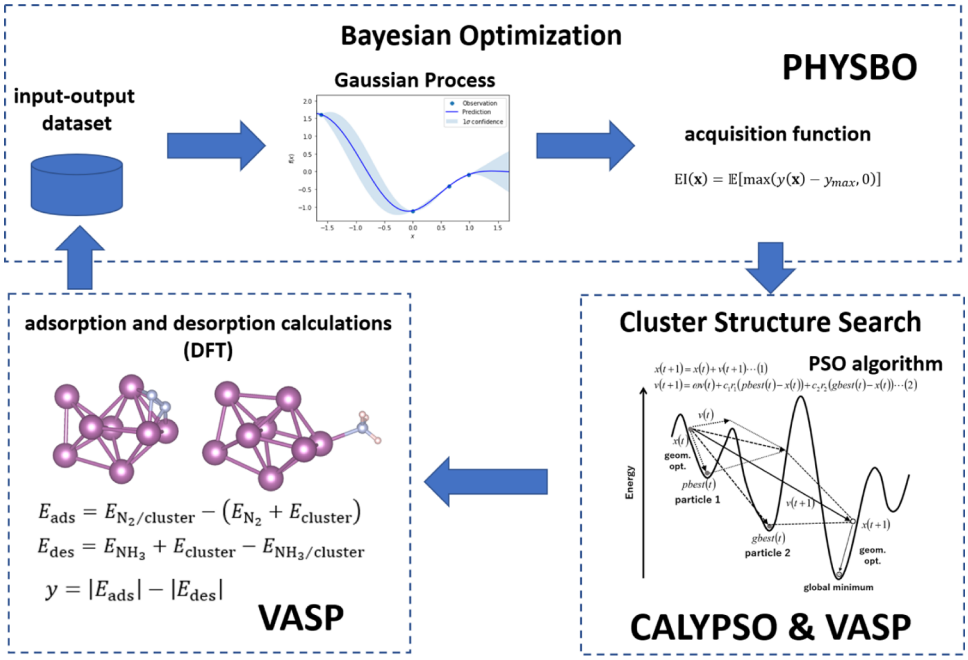

Figure 6. Schematic diagram representing the flow of cluster catalyst search conducted in this study.

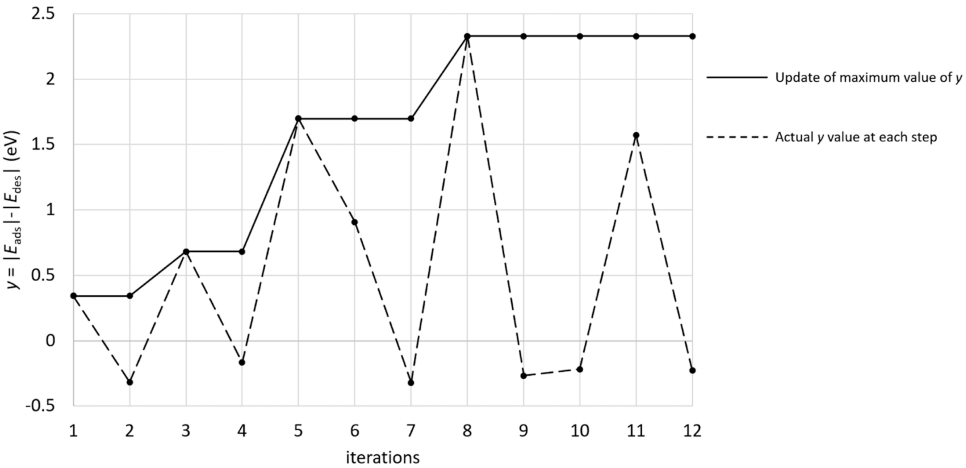

Figure 7. How the maximum value of y, a measure of catalytic activity, is updated as iteration progresses (solid line). The dashed line shows the evolution of the y value calculated for the metal nanocluster actually proposed by BO at each step.

the neighborhood of the point that tentatively gives the optimal value. Such a process is what is represented by the so-called "exploration−exploitation trade-off."[47,111] In order to maintain this balance properly, the AF must be chosen appropriately. PHYSBO includes methods for calculating AFs called EI (expected improvement), PI (probability of improvement), and TS (Thompson sampling).[100]

EI was used as the AF in this study because it offers a good balance between exploration and exploitation and is a common AF used in BO of material product design.[46] EI is probably the most frequently used of the three AFs.[47,111,112] EI is the expected value of how much y_{max}, the maximum value of y currently available, will be updated when $\mathbf{x}$ is observed, and is defined as[93,113]

$$EI(\mathbf{x}) = \mathbb{E}[\max(y(\mathbf{x}) - y_{max}, 0)] \quad (11)$$

At the next observation point suggested by the AF, DFT calculations are performed, and y is determined. The results are then added to the series of equations from eqs 6 to 10. This increases the dimensions of $\mathbf{k}$ and $\mathbf{K}$. The AF is then updated, and we are led to the next search location. This is repeated.

It will be useful here to provide a framework of how we proceeded with this study. Figure 6 shows the scheme. Our study consists of three main components: first, BO, which was performed using PHYSBO as detailed above; second, cluster structure exploration using PSO, which was performed using a combination of CALYPSO (crystal structure analysis by particle swarm optimization)[114−116] and VASP (Vienna Ab initio Simulation Package);[117−120] and third, evaluation of the catalytic activity of metal nanoclusters using DFT calculations, which was performed using VASP. Detailed information on each part, including setting up detailed calculation conditions, can be found in Section 4 at the end of this paper.

2.7. Results of BO. Let us see how the optimization of the metal nanocluster catalyst by BO proceeded. Figure 7 shows the update of the maximum value of the objective function y.

https://doi.org/10.1021/acsomega.3c03456
ACS Omega 2023, 8, 30335−30348

We can see that once every 2 or 3 times, the update of the maximum value occurred. However, after the eighth cycle, the maximum value was not updated for five consecutive cycles. Since the computational cost of running one of the cycles shown in Figure 6 is prohibitive, we decided to terminate our search here.

Let us see which metal nanocluster was actually proposed in each step of the BO. Table 2 summarizes the metal nanocluster proposed at each step. There are also shown the calculated E_{ads} and E_{des} values for each metal cluster. It can be read from these data that large values of y are often the result of large absolute values of E_{ads}. Calculating unbiased variance for the E_{ads} and E_{des} values listed in Table 2 yielded values of 0.64 for the former and 0.08 for the latter. In other words, E_{ads} has a larger variance, suggesting that the variation in y is more influenced by the variation in E_{ads} than by that in E_{des}.

Table 2. The Metal Nanocluster Proposed in Each Step of the BO Cycle, the E_{ads} and E_{des} Values Calculated for Them, and the Value of the Index of Catalytic Activity y Calculated from Them[a]

iterations	metal nanoclusters	E_{ads} (eV)	E_{des} (eV)	y (eV)
1	V_8	−1.32	0.98	0.34
2	Os_6	−1.36	1.67	−0.32
3	Nd_{10}	−1.55	0.87	0.68
4	Ir_9	−1.23	1.40	−0.17
5	Pr_9	−2.41	0.71	1.70
6	La_9	−1.74	0.83	0.91
7	Nb_{10}	−0.73	1.06	−0.32
8	Ti_8	−3.21	0.88	2.33
9	V_{10}	−0.69	0.96	−0.27
10	W_5	−1.07	1.29	−0.22
11	Hf_4	−2.39	0.82	1.57
12	Lu_4	−0.58	0.81	−0.23

[a]All numbers are rounded to two decimal places. y was calculated on the data before rounding, and the result is rounded to two decimal places.

In Section 2.2, we introduced the objective function y. At that time, we did not have reliable information on the variation of E_{ads} and E_{des}, so we treated their contributions as equal. However, to make the resulting contributions of both equal, we may be required to define y with a weighting that takes their variance into account. Addressing such issues remains a challenge for the future.

The best metal nanocluster found in the process of BO is Ti_8. It was found in the 8th BO cycle. After 5 clusters had already been computed for initial data construction, 8 clusters were computed as dictated by BO, and we arrived at Ti_8, achieving our goal by actually computing only 13 clusters out of 308 candidates. This clearly shows the advantage of BO over standard combinatorial approaches. It is interesting to note that for Ti-containing species, Shima and co-workers reported that a trinuclear Ti hydride complex induced N_2 cleavage and partial hydrogenation.[121] The adsorption structures of N_2 and NH_3 on it are shown in Figure 8; the N−N bond is 1.38 Å, suggesting that N_2 is substantially activated as the result of adsorption. The distance between NH_3 and the cluster is also very long at 2.28 Å, suggesting that ammonia is easily desorbed from the cluster. The optimized structure of Ti_8 in Figure 8 seems to be similar to the DFT-based one reported by Lazauskas and co-workers.[122] The index of catalytic activity for

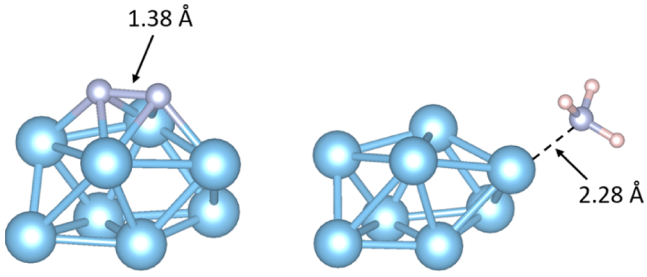

Figure 8. Optimized adsorption structures of N_2 and NH_3 on Ti_8. Selected bond distances are shown.

Ti_8 was as high as 2.33, but could not exceed that for Sc_8, which happened to be included in the initial data. However, Figure 7 shows that the maximum value of y is steadily being updated, suggesting that BO itself is working well. Several interpretations may be possible for this result. For example, one might conclude that Sc_8 was the best catalyst after all, since Figure 7 suggests that no further improvement in y value is expected as the BO cycle progresses. Alternatively, a few more steps of the BO cycle might have found a catalyst with a y value higher than Sc_8. But there would be no end to it. This relates to the difficult question of at what step the BO cycle should be stopped. If the cost of each step is small, it is possible to run many BO cycles, but if the cost of each step is very high, as in this study, the trial must be terminated as early as possible.

As described above, Ti_8 is one of the promising metal clusters as a candidate catalyst for ammonia synthesis. However, this BO study does not take into account the stability of the metal cluster. Hopefully, it is possible to set up an objective function that includes stability. That is left as a future issue. Since there is a previous study on the stability of Ti_n clusters,[123] we would like to build on it to discuss the stability of the Ti cluster. In Sakurai et al.'s study,[123] time-of-flight (TOF) mass spectra showed that the TOF intensities at n = 7, 13, and 15 (so-called magic numbers) were much higher than those at the neighboring n values such as n = 8. The magic-number clusters have large Ti−Ti bond energies, which can be associated with high symmetrical geometries (pentagonal bipyramid for Ti_7, icosahedron for Ti_{13}, and bcc structure units for Ti_{15}). As such, the preparation of the Ti_8 cluster could be difficult because Ti_8 is likely to lose one Ti atom to give Ti_7. Therefore, we also investigated the catalytic activity of Ti_7. The adsorption structures of N_2 and NH_3 on Ti_7 are shown in SI, and it is clear that the binding strength of Ti_7 to NH_3 is strong. Therefore, even if NH_3 is formed on its surface, it is expected to be difficult to desorb. After all, stabilizing Ti_8 without loss of catalytic activity seems to be the most promising strategy. There has also been much research on the stabilization of metal clusters with polymers and dendrimers.[29,124]

We performed BO and consequently performed calculations for the 12 metal clusters, as shown in Table 2. Since there may be more than one possible adsorption site per metal cluster, the pairs of E_{ads} and E_{des} we calculated are actually more than 12. A combined data set of all of the data from the results of those calculations is shown in Figure 9. Note the region enclosed by the dashed line in this figure; as the absolute value of E_{ads} increases, so does E_{des}. This means that metal clusters that strongly adsorb N_2 also strongly adsorb NH_3 in the same way. This is inferred from the so-called scaling relation[125−127] and is considered a natural result. A catalyst must strongly

https://doi.org/10.1021/acsomega.3c03456
ACS Omega 2023, 8, 30335−30348

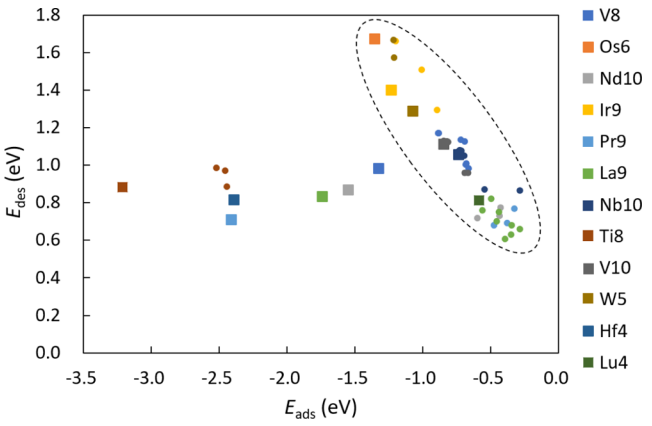

Figure 9. Correlation between E_{ads} and E_{des} values calculated for all metal nanoclusters investigated in the course of BO. The E_{ads} and E_{des} pair that gives the largest y value in each cluster is indicated by the filled square marker. Others are indicated by filled circle markers.

adsorb reactants, but on the other hand, it must also effectively release products. In other words, it is crucial to break the trade-off that usually exists between adsorption of reactants and desorption of products. The dashed area truly reflects such a trade-off.

Let us focus on the region not enclosed by the dashed line in Figure 9. The metal nanoclusters in that region exhibit an interesting property: as the absolute value of E_{ads} increases, the value of E_{des} hardly changes. In this region, the trade-off between adsorption and desorption is broken. Since the best catalyst is one that strongly binds N_2 but weakly binds NH_3, we would expect it to be as far to the lower left as possible in this scatter plot. We can then conclude that Ti_8 is the best in this diagram.

3. CONCLUSIONS

In this paper, we present our efforts toward the theoretical design of metal nanocluster catalysts for efficient ammonia synthesis. We tackled mainly three problems that stand in the way of this task using computational methods. The first problem was how to define a measure of the catalytic activity required for the catalyst for ammonia synthesis. For an optimal catalyst, it is necessary to promote both the adsorption of reactant (N_2) and desorption of product (NH_3), and we proposed to use the difference between the absolute values of the adsorption energy of N_2 and the absolute value of the desorption barrier of NH_3 as a measure of catalytic activity. These energy values were evaluated using first-principles calculations. The second problem was the large number of candidate metal nanoclusters. The combinations of metal elements and the number of metal atoms that make up the metal nanocluster are enormous, and it is necessary to effectively choose the best one (the one with the highest measure of catalytic activity). BO was utilized for this purpose. The third problem was the large number of isomers of the metal nanocluster. As the number of metal atoms constituting the metal nanocluster increases, the number of isomers increases exponentially. It is necessary to identify the thermodynamically stable cluster structure effectively. To solve this problem, we utilized PSO, a type of swarm intelligence, in combination with first-principles calculations. By utilizing the three tools of first-principles calculations, BO, and PSO, we succeeded in obtaining the Ti_8 nanocluster as a catalyst candidate. In the N_2 adsorption structure on Ti_8, the N−N bond is elongated, indicating that the N_2 molecule is activated. In the NH_3 adsorption structure, the distance between NH_3 and the cluster is elongated, indicating that NH_3 is likely to easily be desorbed. However, the measure of catalytic activity calculated for Ti_8 could not exceed the value calculated for Sc_8, which happened to be included in the initial data for BO. As a result, we found Ti_8 through BO, and Sc_8 accidentally. However, BO also brought another important discovery. Among the metal nanoclusters found in the BO process of this study, there were several candidates that broke the general trade-off that surfaces that strongly adsorb reactants also strongly adsorb products.

4. COMPUTATIONAL METHODS

4.1. Exploration of Metal Nanocluster Structures. CALYPSO v.5.0[114−116] was used to search for the most stable structure of each metal nanocluster; the population of each generation generated by CALYPSO was set to 20. Sixteen of these were generated using PSO, and the remaining four were randomly generated to ensure diversity. To ensure that metastable structures are also searched for, a local PSO algorithm with Metropolis criterion was employed.[62] We decided to search for up to 70 generations, but if the magnitude of change in the energy update of the most stable cluster was less than 0.001 eV for 10 consecutive generations, the calculation was terminated at that point.

The initial structures of the metal nanoclusters generated by CALYPSO were optimized using VASP 5.4.4. VASP can only optimize structures with imposed periodic boundary conditions. Since nanoclusters are not periodic systems, calculations were performed with a nanocluster placed within a large orthorhombic unit cell surrounded by a vacuum layer. The distance between the nanocluster and the periodic images in the vicinity was set longer than 15 Å. The need for a distance greater than 15 Å is based on the literature.[67−69] The results of the literature survey,[128−130] which shows that a vacuum layer thicker than 15 Å is generally introduced when building a slab model, also support the validity of setting this distance. We refer to previous studies for the calculation of clusters using such a method.[67−69,131−133] In the VASP calculation, the Perdew−Burke−Ernzerhof (PBE) functional,[134] a generalized gradient approximation (GGA), was used. Grimme's D2 dispersion correction was applied.[135] The cutoff energy was set to 300 eV, and the energy convergence condition in the self-consistent field (SCF) cycle was set to 1.0×10^{-3} eV. Spin-polarized calculations (collinear) were performed. We have verified the validity of spin polarization calculations using VASP in our previous work.[68] The magnetic moments calculated for all optimized metal clusters are tabulated in the SI. The convergence condition for geometry optimization was set to 1.0×10^{-2} eV. The abovementioned computational conditions are set slightly loose. This is to accelerate the structure search.

After the structural search was completed, more rigorous computational conditions were applied to the most stable metal nanocluster structures found, and the cluster structures were re-optimized. The modifications to the calculation conditions are as follows. The cutoff energy was increased to 500 eV, and the convergence condition for the SCF cycle was set to 1.0×10^{-6} eV. The interatomic force was adopted as the convergence condition for geometry optimization, and its value

https://doi.org/10.1021/acsomega.3c03456
ACS Omega 2023, 8, 30335−30348

was set to 0.05 eV/Å. The other calculation conditions remained unchanged.

4.2. Evaluation of Catalytic Activity. Calculations of the adsorption and desorption energies of N_2 and NH_3 for the evaluation of the catalytic activity were based on eqs 2 and 3, respectively. Optimizations of the adsorption structures of these molecules were performed using VASP. Adsorption structures at all symmetrically distinct metal atom sites were investigated. Thus, multiple adsorption structures were obtained for each cluster. The lowest energy among them was selected as the stable structure. One could do cluster expansion and machine learning approaches to determine adsorption sites on clusters that are more heterogeneous and hence challenging than elemental metal surfaces.[136] Catalysts should be covered by reagents with higher coverage, but due to limited computational costs, the investigation was limited to the dilution limit.

The PBE functional was used, Grimme's D2 dispersion correction was applied, the cutoff energy was set to 500 eV, and the energy convergence condition in the SCF cycle was 1.0×10^{-6} eV. Spin polarization was included within the calculations being performed at the γ point. The force acting between atoms was adopted as the convergence condition for structural optimization, and its value was set to 0.05 eV/Å. These conditions are the same as the "rigorous" condition setting described above. The optimized structures were visualized by VESTA.[137]

4.3. Execution of BO. PHYSBO, a Python 3 library, was used to perform the BO. The RBF kernel was used as the kernel function and EI as the AF. The optimization was terminated when the best objective function value was not updated for five consecutive runs.

■ ASSOCIATED CONTENT

Supporting Information

The Supporting Information is available free of charge at https://pubs.acs.org/doi/10.1021/acsomega.3c03456.

Complete list of metal clusters calculated in this study, their magnetic moments, optimized adsorption structures of N_2 and NH_3 on Ti_7, and atomic coordinates of DFT-optimized structures (PDF)

■ AUTHOR INFORMATION

Corresponding Author

Yuta Tsuji − *Faculty of Engineering Sciences, Kyushu University, Kasuga, Fukuoka 816-8580, Japan;* orcid.org/0000-0003-4224-4532; Email: tsuji.yuta.955@m.kyushu-u.ac.jp

Authors

Yuta Yoshioka − *Institute for Materials Chemistry and Engineering and IRCCS, Kyushu University, Nishi-ku, Fukuoka 819-0395, Japan*

Kazuki Okazawa − *Institute for Materials Chemistry and Engineering and IRCCS, Kyushu University, Nishi-ku, Fukuoka 819-0395, Japan;* orcid.org/0000-0001-6515-4367

Kazunari Yoshizawa − *Institute for Materials Chemistry and Engineering and IRCCS, Kyushu University, Nishi-ku, Fukuoka 819-0395, Japan;* orcid.org/0000-0002-6279-9722

Complete contact information is available at: https://pubs.acs.org/10.1021/acsomega.3c03456

Notes

The authors declare no competing financial interest.

■ ACKNOWLEDGMENTS

This work was supported by KAKENHI grants (number JP21K04996 and JP22H00335) from the Japan Society for the Promotion of Science (JSPS) and the Ministry of Education, Culture, Sports, Science and Technology of Japan (MEXT) through the MEXT projects Integrated Research Consortium on Chemical Sciences, Cooperative Research Program of Network Joint Research Center for Materials and Devices and Elements Strategy Initiative to Form Core Research Center, and by JST-CREST JPMJCR15P5 and JST, the establishment of university fellowships toward the creation of science technology innovation JPMJFS2132. The authors are grateful for a JSPS Grant-in-Aid for Scientific Research on Innovative Areas (Discrete Geometric Analysis for Materials Design, grant number JP20H04643) and a Grant-in-Aid for Transformative Research Areas (A) "Supra-ceramics" (grant number JP22H05146). Y.T. acknowledges JACI Prize for Encouraging Young Researcher. The computations in this work were performed using the computer facilities at the Research Institute for Information Technology, Kyushu University, and at the Supercomputer Center, the Institute for Solid State Physics, the University of Tokyo.

■ REFERENCES

(1) Haber, F. *The Synthesis of Ammonia from its Elements*; Nobel Lecture in Chemistry, June 2, 1920.

(2) Liu, H. Ammonia Synthesis Catalyst 100 Years: Practice, Enlightenment and Challenge. *Chin. J. Catal.* **2014**, *35*, 1619−1640.

(3) Erisman, J. W.; Sutton, M. A.; Galloway, J.; Klimont, Z.; Winiwarter, W. How a Century of Ammonia Synthesis Changed the World. *Nat. Geosci.* **2008**, *1*, 636−639.

(4) McQuarrie, D.; Simon, J. *Physical Chemistry: A Molecular Approach*; University Science Books: Sausalito, CA, 1997.

(5) Housecroft, C. E.; Sharpe, A. G. *Inorganic Chemistry*, 3rd ed.; Pearson Education Ltd.: Harlow, 2008.

(6) Cotton, F. A.; Wilkinson, G.; Gaus, P. L. *Basic Inorganic Chemistry*; 4th ed.; Wiley: New York, 1995.

(7) Kyriakou, V.; Garagounis, I.; Vourros, A.; Vasileiou, E.; Stoukides, M. An Electrochemical Haber-Bosch Process. *Joule* **2020**, *4*, 142−158.

(8) Buscagan, T. M.; Rees, D. C. Rethinking the Nitrogenase Mechanism: Activating the Active Site. *Joule* **2019**, *3*, 2662−2678.

(9) Tanaka, H.; Nishibayashi, Y.; Yoshizawa, K. Interplay between Theory and Experiment for Ammonia Synthesis Catalyzed by Transition Metal Complexes. *Acc. Chem. Res.* **2016**, *49*, 987−995.

(10) Kitano, M.; Kanbara, S.; Inoue, Y.; Kuganathan, N.; Sushko, P. V.; Yokoyama, T.; Hara, M.; Hosono, H. Electride Support Boosts Nitrogen Dissociation Over Ruthenium Catalyst and Shifts the Bottleneck in Ammonia Synthesis. *Nat. Commun.* **2015**, *6*, No. 6731.

(11) Kitano, M.; Inoue, Y.; Yamazaki, Y.; Hayashi, F.; Kanbara, S.; Matsuishi, S.; Yokoyama, T.; Kim, S.-W.; Hara, M.; Hosono, H. Ammonia Synthesis Using a Stable Electride as an Electron Donor and Reversible Hydrogen Store. *Nat. Chem.* **2012**, *4*, 934−940.

(12) Lu, Y. F.; Li, J.; Tada, T.; Toda, Y.; Ueda, S.; Yokoyama, T.; Kitano, M.; Hosono, H. Water Durable Electride Y_5Si_3: Electronic Structure and Catalytic Activity for Ammonia Synthesis. *J. Am. Chem. Soc.* **2016**, *138*, 3970−3973.

(13) Kobayashi, Y.; Tang, Y.; Kageyama, T.; Yamashita, H.; Masuda, N.; Hosokawa, S.; Kageyama, H. Titanium-Based Hydrides as Heterogeneous Catalysts for Ammonia Synthesis. *J. Am. Chem. Soc.* **2017**, *139*, 18240−18246.

(14) Cao, Y.; Saito, A.; Kobayashi, Y.; Ubukata, H.; Tang, Y.; Kageyama, H. Vanadium Hydride as an Ammonia Synthesis Catalyst. *ChemCatChem* **2021**, *13*, 191−195.
(15) Tsuji, Y.; Okazawa, K.; Kobayashi, Y.; Kageyama, H.; Yoshizawa, K. Electronic Origin of Catalytic Activity of TiH_2 for Ammonia Synthesis. *J. Phys. Chem. C* **2021**, *125*, 3948−3960.
(16) Ye, T. N.; Park, S. W.; Lu, Y.; Li, J.; Sasase, M.; Kitano, M.; Tada, T.; Hosono, H. Vacancy-Enabled N_2 Activation for Ammonia Synthesis on an Ni-Loaded Catalyst. *Nature* **2020**, *583*, 391−395.
(17) Kitano, M.; Kujirai, J.; Ogasawara, K.; Matsuishi, S.; Tada, T.; Abe, H.; Niwa, Y.; Hosono, H. Low-Temperature Synthesis of Perovskite Oxynitride-Hydrides as Ammonia Synthesis Catalysts. *J. Am. Chem. Soc.* **2019**, *141*, 20344−20353.
(18) Hagen, S.; Barfod, R.; Fehrmann, R.; Jacobsen, C. J. H.; Teunissen, H. T.; Chorkendorff, I. Ammonia Synthesis with Barium-Promoted Iron-Cobalt Alloys Supported on Carbon. *J. Catal.* **2003**, *214*, 327−335.
(19) Okazawa, K.; Tsuji, Y.; Kurino, K.; Yoshida, M.; Amamoto, Y.; Yoshizawa, K. Exploring the Optimal Alloy for Nitrogen Activation by Combining Bayesian Optimization with Density Functional Theory Calculations. *ACS Omega* **2022**, *7*, 45403−45408.
(20) Ogawa, T.; Kobayashi, Y.; Mizoguchi, H.; Kitano, M.; Abe, H.; Tada, T.; Toda, Y.; Niwa, Y.; Hosono, H. High Electron Density on Ru in Intermetallic YRu_2: The Application to Catalyst for Ammonia Synthesis. *J. Phys. Chem. C* **2018**, *122*, 10468−10475.
(21) Armbrüster, M. Intermetallic Compounds in Catalysis − A Versatile Class of Materials Meets Interesting Challenges. *Sci. Technol. Adv. Mater.* **2020**, *21*, 303−322.
(22) Marakatti, V. S.; Gaigneaux, E. M. Recent Advances in Heterogeneous Catalysis for Ammonia Synthesis. *ChemCatChem* **2020**, *12*, 5838−5857.
(23) Wang, Q.; Guo, J.; Chen, P. Recent Progress Towards Mild-Condition Ammonia Synthesis. *J. Energy Chem.* **2019**, *36*, 25−36.
(24) Zhang, L.; Wang, Y.; Niu, Z.; Chen, J. Single Atoms on Graphene for Energy Storage and Conversion. *Small Methods* **2019**, *3*, No. 1800443.
(25) Lu, Y. Z.; Chen, W. Sub-Nanometre Sized Metal Clusters: From Synthetic Challenges to the Unique Property Discoveries. *Chem. Soc. Rev.* **2012**, *41*, 3594−3623.
(26) Gao, X. H.; Yu, G. T.; Zheng, L. R.; Zhang, C. M.; Li, H.; Wang, T.; An, P. D.; Liu, M.; Qiu, X. Q.; Chen, W.; Chen, W. Strong Electron Coupling from the Sub-Nanometer Pd Clusters Confined in Porous Ceria Nanorods for Highly Efficient Electrochemical Hydrogen Evolution Reaction. *ACS Appl. Mater. Interfaces* **2019**, *2*, 966−973.
(27) Imaoka, T.; Yamamoto, K. Wet-Chemical Strategy for Atom-Precise Metal Cluster Catalysts. *Bull. Chem. Soc. Jpn.* **2019**, *92*, 941−948.
(28) Lang, S. M.; Bernhardt, T. M. Gas Phase Metal Cluster Model Systems for Heterogeneous Catalysis. *Phys. Chem. Chem. Phys.* **2012**, *14*, 9255−9269.
(29) Yamazoe, S.; Koyasu, K.; Tsukuda, T. Nonscalable Oxidation Catalysis of Gold Clusters. *Acc. Chem. Res.* **2014**, *47*, 816−824.
(30) Ferrando, R.; Jellinek, J.; Johnston, R. L. Nanoalloys: From Theory to Applications of Alloy Clusters and Nanoparticles. *Chem. Rev.* **2008**, *108*, 845−910.
(31) Lu, Z.; Yin, Y. Colloidal Nanoparticle Clusters: Functional Materials by Design. *Chem. Soc. Rev.* **2012**, *41*, 6874−6887.
(32) Dai, Y.; Wang, Y.; Liu, B.; Yang, Y. Metallic Nanocatalysis: An Accelerating Seamless Integration with Nanotechnology. *Small* **2015**, *11*, 268−289.
(33) Chen, Y.; Wang, H.; Liu, C.-J.; Zeng, Z.; Zhang, H.; Zhou, C.; Jia, X.; Yang, Y. Formation of Monometallic Au and Pd and Bimetallic Au−Pd Nanoparticles Confined in Mesopores via Ar Glow-Discharge Plasma Reduction and Their Catalytic Applications in Aerobic Oxidation of Benzyl Alcohol. *J. Catal.* **2012**, *289*, 105−117.
(34) Li, L.; Jiang, Y.-F.; Zhang, T.; Cai, H.; Zhou, Y.; Lin, B.; Lin, X.; Zheng, Y.; Zheng, L.; Wang, X.; Xu, C.-Q.; Au, C.; Jiang, L.; Li, J. Size Sensitivity of Supported Ru Catalysts for Ammonia Synthesis: From Nanoparticles to Subnanometric Clusters and Atomic Clusters. *Chem* **2022**, *8*, 749−768.
(35) Liu, J.-C.; Ma, X.-L.; Li, Y.; Wang, Y.-G.; Xiao, H.; Li, J. Heterogeneous Fe_3 Single-Cluster Catalyst for Ammonia Synthesis via an Associative Mechanism. *Nat. Commun.* **2018**, *9*, No. 1610.
(36) Ma, X.-L.; Liu, J.-C.; Xiao, H.; Li, J. Surface Single-Cluster Catalyst for N_2-to-NH_3 Thermal Conversion. *J. Am. Chem. Soc.* **2018**, *140*, 46−49.
(37) Peng, X.; Cai, H.; Zhou, Y.; Ni, J.; Wang, X.; Lin, B.; Lin, J.; Zheng, L.; Au, C.-t.; Jiang, L. Studies of a Highly Active Cobalt Atomic Cluster Catalyst for Ammonia Synthesis. *ACS Sustainable Chem. Eng.* **2022**, *10*, 1951−1960.
(38) Takahashi, K.; Takahashi, L.; Miyazato, I.; Fujima, J.; Tanaka, Y.; Uno, T.; Satoh, H.; Ohno, K.; Nishida, M.; Hirai, K.; et al. The Rise of Catalyst Informatics: Towards Catalyst Genomics. *ChemCatChem* **2019**, *11*, 1146−1152.
(39) Takahashi, K.; Ohyama, J.; Nishimura, S.; Fujima, J.; Takahashi, L.; Uno, T.; Taniike, T. Catalysts Informatics: Paradigm Shift towards Data-Driven Catalyst Design. *Chem. Commun.* **2023**, *59*, 2222−2238.
(40) Toyao, T.; Maeno, Z.; Takakusagi, S.; Kamachi, T.; Takigawa, I.; Shimizu, K. I. Machine Learning for Catalysis Informatics: Recent Applications and Prospects. *ACS Catal.* **2020**, *10*, 2260−2297.
(41) Tsuji, Y.; Yoshida, M.; Yoshizawa, K.; Kamachi, T. Concepts of Computational Approach to Explore Heterogeneous Catalysts for Direct Methane Conversion. *ChemCatChem* **2023**, *15*, No. e202201488.
(42) Kang, J.; Noh, S. H.; Hwang, J.; Chun, H.; Kim, H.; Han, B. First-Principles Database Driven Computational Neural Network Approach to the Discovery of Active Ternary Nanocatalysts for Oxygen Reduction Reaction. *Phys. Chem. Chem. Phys.* **2018**, *20*, 24539−24544.
(43) Takahashi, K.; Takahashi, L.; Le, S. D.; Kinoshita, T.; Nishimura, S.; Ohyama, J. Synthesis of Heterogeneous Catalysts in Catalyst Informatics to Bridge Experiment and High-Throughput Calculation. *J. Am. Chem. Soc.* **2022**, *144*, 15735−15744.
(44) Toyao, T.; Suzuki, K.; Kikuchi, S.; Takakusagi, S.; Shimizu, K. I.; Takigawa, I. Toward Effective Utilization of Methane: Machine Learning Prediction of Adsorption Energies on Metal Alloys. *J. Phys. Chem. C* **2018**, *122*, 8315−8326.
(45) Frazier, P. I. A tutorial on Bayesian optimization. 2018, arXiv:1807.02811. arXiv.org e-Print archive. https://arxiv.org/abs/1807.02811.
(46) Wang, K.; Dowling, A. W. Bayesian Optimization for Chemical Products and Functional Materials. *Curr. Opin. Chem. Eng.* **2022**, *36*, No. 100728.
(47) Hashimoto, W.; Tsuji, Y.; Yoshizawa, K. Optimization of Work Function via Bayesian Machine Learning Combined with First-Principles Calculation. *J. Phys. Chem. C* **2020**, *124*, 9958−9970.
(48) Turner, R.; Eriksson, D.; Mccourt, M.; Kiili, J.; Xu, V. Z.; Escalante, H. J.; Hofmann, K. Bayesian Optimization Is Superior to Random Search for Machine Learning Hyperparameter Tuning: Analysis of the Black-Box Optimization Challenge 2020. *PMLR* **2021**, 3−26.
(49) Kitamura, Y.; Toshima, H.; Inokuchi, A.; Tanaka, D. Bayesian Optimization of the Composition of the Lanthanide Metal-Organic Framework MIL-103 for White-Light Emission. *Mol. Syst. Des. Eng.* **2023**, *8*, 431−435.
(50) Hernández-Lobato, J. M.; Requeima, J.; Pyzer-Knapp, E. O.; Aspuru-Guzik, A. In *Parallel and Distributed Thompson Sampling for Large-Scale Accelerated Exploration of Chemical Space*, Proceedings of the 34th International Conference on Machine Learning, Sydney, Australia, 2017.
(51) Goel, M.; Aggarwal, R.; Sridharan, B.; Pal, P. K.; Priyakumar, U. D. Efficient and Enhanced Sampling of Drug-Like Chemical Space for Virtual Screening and Molecular Design Using Modern Machine Learning Methods. *Wiley Interdiscip. Rev.: Comput. Mol. Sci.* **2022**, *13*, No. e1637.

https://doi.org/10.1021/acsomega.3c03456
ACS Omega 2023, 8, 30335−30348

(52) Garcia-Santiago, X.; Schneider, P. I.; Rockstuhl, C.; Burger, S. Shape Design of a Reflecting Surface Using Bayesian Optimization. *J. Phys.: Conf. Ser.* **2018**, *963*, No. 012003.
(53) Schneider, P.-I.; Santiago, X. G.; Rockstuhl, C.; Burger, S. Global Optimization of Complex Optical Structures Using Bayesian Optimization Based on Gaussian Processes. *Proc. SPIE* **2017**, *103350*, No. 103350O.
(54) Pedersen, J. K.; Clausen, C. M.; Krysiak, O. A.; Xiao, B.; Batchelor, T. A. A.; Löffler, T.; Mints, V. A.; Banko, L.; Arenz, M.; Savan, A.; Schuhmann, W.; Ludwig, A.; Rossmeisl, J. Bayesian Optimization of High-Entropy Alloy Compositions for Electrocatalytic Oxygen Reduction. *Angew. Chem., Int. Ed.* **2021**, *60*, 24144−24152.
(55) Nugraha, A. S.; Lambard, G.; Na, J.; Hossain, M. S. A.; Asahi, T.; Chaikittisilp, W.; Yamauchi, Y. Mesoporous Trimetallic PtPdAu Alloy Films toward Enhanced Electrocatalytic Activity in Methanol Oxidation: Unexpected Chemical Compositions Discovered by Bayesian Optimization. *J. Mater. Chem. A* **2020**, *8*, 13532−13540.
(56) Nagai, K.; Osa, T.; Inoue, G.; Tsujiguchi, T.; Araki, T.; Kuroda, Y.; Tomizawa, M.; Nagato, K. Sample-Efficient Parameter Exploration of the Powder Film Drying Process Using Experiment-Based Bayesian Optimization. *Sci. Rep.* **2022**, *12*, No. 1615.
(57) Zuo, Y.; Qin, M.; Chen, C.; Ye, W.; Li, X.; Luo, J.; Ong, S. P. Accelerating Materials Discovery with Bayesian Optimization and Graph Deep Learning. *Mater. Today* **2021**, *51*, 126−135.
(58) Seko, A.; Togo, A.; Hayashi, H.; Tsuda, K.; Chaput, L.; Tanaka, I. Prediction of Low-Thermal-Conductivity Compounds with First-Principles Anharmonic Lattice-Dynamics Calculations and Bayesian Optimization. *Phys. Rev. Lett.* **2015**, *115*, No. 205901.
(59) Stillinger, F. H. Exponential Multiplicity of Inherent Structures. *Phys. Rev. E* **1999**, *59*, 48−51.
(60) Lyakhov, A. O.; Oganov, A. R.; Stokes, H. T.; Zhu, Q. New Developments in Evolutionary Structure Prediction Algorithm USPEX. *Comput. Phys. Commun.* **2013**, *184*, 1172−1182.
(61) Daven, D. M.; Tit, N.; Morris, J. R.; Ho, K. M. Structural Optimization of Lennard-Jones Clusters by a Genetic Algorithm. *Chem. Phys. Lett.* **1996**, *256*, 195−200.
(62) Lv, J.; Wang, Y.; Zhu, L.; Ma, Y. Particle-Swarm Structure Prediction on Clusters. *J. Chem. Phys.* **2012**, *137*, No. 084104.
(63) Wang, H.; Wang, Y.; Lv, J.; Li, Q.; Zhang, L.; Ma, Y. CALYPSO Structure Prediction Method and Its Wide Application. *Comput. Mater. Sci.* **2016**, *112*, 406−415.
(64) Hodgson, R. J. W. Particle Swarm Optimization Applied to the Atomic Cluster Optimization Problem. *Proc. Genet. Evol. Comp. Conf.* **2002**, 68−73.
(65) Call, S. T.; Zubarev, D. Y.; Boldyrev, A. I. Global Minimum Structure Searches via Particle Swarm Optimization. *J. Comput. Chem.* **2007**, *28*, 1177−1186.
(66) Eberhart, R.; Kennedy, J. A New Optimizer Using Particle Swarm Theory. *Proc. Int. Symp. - Micro Mach. Hum. Sci.* **1995**, 39−43.
(67) Tsuji, Y.; Yoshizawa, K. From Infection Clusters to Metal Clusters: Significance of the Lowest Occupied Molecular Orbital (LOMO). *ACS Omega* **2021**, *6*, 1339−1351.
(68) Hori, M.; Tsuji, Y.; Yoshizawa, K. Bonding of C_1 Fragments on Metal Nanoclusters: A Search for Methane Conversion Catalysts with Swarm Intelligence. *Phys. Chem. Chem. Phys.* **2021**, *23*, 14004−14015.
(69) Tsuji, Y.; Yoshioka, Y.; Hori, M.; Yoshizawa, K. Exploring Metal Cluster Catalysts Using Swarm Intelligence: Start with Hydrogen Adsorption. *Top. Catal.* **2022**, *65*, 215−227.
(70) Dybkær, R. The Tortuous Road to the Adoption of katal for the Expression of Catalytic Activity by the General Conference on Weights and Measures. *Clin. Chem.* **2002**, *48*, 586−590.
(71) Feng, Y. Z.; Rao, P. M.; Kim, D. R.; Zheng, X. L. Methane Oxidation over Catalytic Copper Oxides Nanowires. *Proc. Combust. Inst.* **2011**, *33*, 3169−3175.
(72) Wei, Y.; Jiang, W.; Liu, Y.; Bai, X.; Hao, D.; Ni, B. J. Recent Advances in Photocatalytic Nitrogen Fixation and Beyond. *Nanoscale* **2022**, *14*, 2990−2997.
(73) Xu, T.; Liang, J.; Li, S.; Xu, Z.; Yue, L.; Li, T.; Luo, Y.; Liu, Q.; Shi, X.; Asiri, A. M.; Yang, C.; Sun, X. Recent Advances in Nonprecious Metal Oxide Electrocatalysts and Photocatalysts for N_2 Reduction Reaction under Ambient Condition. *Small Sci.* **2021**, *1*, No. 2000069.
(74) Liu, D.; Chen, M.; Du, X.; Ai, H.; Lo, K. H.; Wang, S.; Chen, S.; Xing, G.; Wang, X.; Pan, H. Development of Electrocatalysts for Efficient Nitrogen Reduction Reaction under Ambient Condition. *Adv. Funct. Mater.* **2021**, *31*, No. 2008983.
(75) Wang, K.; Smith, D.; Zheng, Y. Electron-Driven Heterogeneous Catalytic Synthesis of Ammonia: Current States and Perspective. *Carbon Resour. Convers.* **2018**, *1*, 2−31.
(76) Li, C.; Wang, T.; Gong, J. Alternative Strategies Toward Sustainable Ammonia Synthesis. *Transactions of Tianjin University* **2020**, *26*, 67−91.
(77) Honkala, K.; Hellman, A.; Remediakis, I. N.; Logadottir, A.; Carlsson, A.; Dahl, S.; Christensen, C. H.; Noerskov, J. K. Ammonia Synthesis from First-Principles Calculations. *Science* **2005**, *307*, 555−558.
(78) Ertl, G. Primary Steps in Catalytic Synthesis of Ammonia. *J. Vac. Sci. Technol., A* **1983**, *1*, 1247−1253.
(79) Hammond, G. S. A Correlation of Reaction Rates. *J. Am. Chem. Soc.* **1955**, *77*, 334−338.
(80) Bell, R. P. The Theory of Reactions Involving Proton Transfers. *Proc. R. Soc. London, Ser. A* **1936**, *154*, 414−429.
(81) Evans, M. G.; Polanyi, M. Some Applications of the Transition State Method to the Calculation of Reaction Velocities, Especially in Solution. *Trans. Faraday Soc.* **1935**, *31*, 875−894.
(82) Jacobsen, C. J. H.; Dahl, S.; Clausen, B. S.; Bahn, S.; Logadottir, A.; Nørskov, J. K. Catalyst Design by Interpolation in the Periodic Table: Bimetallic Ammonia Synthesis Catalysts. *J. Am. Chem. Soc.* **2001**, *123*, 8404−8405.
(83) Saidi, W. A.; Shadid, W.; Veser, G. Optimization of High-Entropy Alloy Catalyst for Ammonia Decomposition and Ammonia Synthesis. *J. Phys. Chem. Lett.* **2021**, *12*, 5185−5192.
(84) Zangwill, A. *Physics at Surfaces*; University Press: Cambridge, 1988.
(85) Ertl, G. Reactions at Surfaces from Atoms to Complexity (Nobel Lecture). *Angew. Chem., Int. Ed.* **2008**, *47*, 3524−3535.
(86) Ertl, G.; Weiss, M.; Lee, S. B. Role of Potassium in the Catalytic Synthesis of Ammonia. *Chem. Phys. Lett.* **1979**, *60*, 391−394.
(87) Ye, K.; Hu, M.; Li, Q.-K.; Luo, Y.; Jiang, J.; Zhang, G. Cooperative Single-Atom Active Centers for Attenuating the Linear Scaling Effect in the Nitrogen Reduction Reaction. *J. Phys. Chem. Lett.* **2021**, *12*, 5233−5240.
(88) Zeinalipour-Yazdi, C. D.; Hargreaves, J. S. J.; Catlow, C. R. A. DFT-D3 Study of Molecular N_2 and H_2 Activation on Co_3Mo_3N Surfaces. *J. Phys. Chem. C* **2016**, *120*, 21390−21398.
(89) Che, M. Nobel Prize in Chemistry 1912 to Sabatier: Organic Chemistry or Catalysis? *Catal. Today* **2013**, *218*−*219*, 162−171.
(90) Xu, G.; Cai, C.; Wang, T. Toward Sabatier Optimal for Ammonia Synthesis with Paramagnetic Phase of Ferromagnetic Transition Metal Catalysts. *J. Am. Chem. Soc.* **2022**, *144*, 23089−23095.
(91) Medford, A. J.; Vojvodic, A.; Hummelshøj, J. S.; Voss, J.; Abild-Pedersen, F.; Studt, F.; Bligaard, T.; Nilsson, A.; Nørskov, J. K. From the Sabatier Principle to a Predictive Theory of Transition-Metal Heterogeneous Catalysis. *J. Catal.* **2015**, *328*, 36−42.
(92) Gao, W.; Li, X.; Luo, S.; Luo, Z.; Zhang, X.; Huang, R.; Luo, M. In Situ Modification of Cobalt on MXene/TiO_2 as Composite Photocatalyst for Efficient Nitrogen Fixation. *J. Colloid Interface Sci.* **2021**, *585*, 20−29.
(93) Motoyama, Y.; Tamura, R.; Yoshimi, K.; Terayama, K.; Ueno, T.; Tsuda, K. Bayesian Optimization Package: PHYSBO. *Comput. Phys. Commun.* **2022**, *278*, No. 108405.
(94) https://www.pasums.issp.u-tokyo.ac.jp/physbo/.
(95) Ueno, T.; Rhone, T. D.; Hou, Z.; Mizoguchi, T.; Tsuda, K. COMBO: An Efficient Bayesian Optimization Library for Materials Science. *Mater. Discovery* **2016**, *4*, 18−21.

https://doi.org/10.1021/acsomega.3c03456
ACS Omega 2023, 8, 30335−30348

(96) Aoyagi, T. Optimization of the Elastic Properties of Block Copolymers Using Coarse-Grained Simulation and an Artificial Neural Network. *Comput. Mater. Sci.* **2022**, *207*, No. 111286.
(97) Matsuda, Y.; Ookawara, S.; Yasuda, T.; Yoshikawa, S.; Matsumoto, H. Framework for Discovering Porous Materials: Structural Hybridization and Bayesian Optimization of Conditional Generative Adversarial Network. *Digit. Chem. Eng.* **2022**, *5*, No. 100058.
(98) Motoyama, Y.; Yoshimi, K.; Mochizuki, I.; Iwamoto, H.; Ichinose, H.; Hoshi, T. Data-Analysis Software Framework 2DMAT and its Application to Experimental Measurements for Two-Dimensional Material Structures. *Comput. Phys. Comm.* **2022**, *280*, No. 108465.
(99) Amamoto, Y. Data-Driven Approaches for Structure-Property Relationships in Polymer Science for Prediction and Understanding. *Polym. J.* **2022**, *54*, 957−967.
(100) PHYSBO Documentation Release 1.0.1. https://www.pasums.issp.u-tokyo.ac.jp/physbo/wp-content/uploads/sites/12/2022/05/physbo_en_v1.0.1.pdf.
(101) Packwood, D. *Bayesian Optimization for Materials Science*; Springer: Singapore, 2017; pp 1−10.
(102) Rupp, M.; Tkatchenko, A.; Müller, K.-R.; von Lilienfeld, O. A. Fast and Accurate Modeling of Molecular Atomization Energies with Machine Learning. *Phys. Rev. Lett.* **2012**, *108*, No. 058301.
(103) Hansen, K.; Montavon, G.; Biegler, F.; Fazli, S.; Rupp, M.; Scheffler, M.; Von Lilienfeld, O. A.; Tkatchenko, A.; Müller, K.-R. Assessment and Validation of Machine Learning Methods for Predicting Molecular Atomization Energies. *J. Chem. Theory Comput.* **2013**, *9*, 3404−3419.
(104) Saidi, W. A.; Shadid, W.; Castelli, I. E. Machine-Learning Structural and Electronic Properties of Metal Halide Perovskites Using a Hierarchical Convolutional Neural Network. *npj Comput. Mater.* **2020**, *6*, No. 36.
(105) Saidi, W. A. Emergence of Local Scaling Relations in Adsorption Energies on High-Entropy Alloys. *npj Comput. Mater.* **2022**, *8*, No. 86.
(106) Tian, F. Y.; Jing, Q.; Wang, Y. X. Structure, Stability, and Magnetism of Sc_nAl (n = 1−8, 12) Clusters: Density-Functional Theory Investigations. *Phys. Rev. A* **2008**, *77*, No. 013202.
(107) Jaque, P.; Toro-Labbé, A. Polarizability of Neutral Copper Clusters. *J. Mol. Model.* **2014**, *20*, 2410.
(108) Carroll, L. L.; Moskaleva, L. V.; de Lara-Castells, M. P. Carbon Vacancy-Assisted Stabilization of Individual Cu_5 Clusters on Graphene. Insights from Ab Initio Molecular Dynamics. *Phys. Chem. Chem. Phys.* **2023**, *25*, 15729−15743.
(109) Shi, Y. L.; Song, B.; Shahbazian-Yassar, R.; Zhao, J.; Saidi, W. A. Experimentally Validated Structures of Supported Metal Nanoclusters on MoS_2. *J. Phys. Chem. Lett.* **2018**, *9*, 2972−2978.
(110) Shi, Y.; Rabbani, M.; Vázquez-Mayagoitia, A.; Zhao, J.; Saidi, W. A. Controlling the Nucleation and Growth of Ultrasmall Metal Nanoclusters with MoS_2 Grain Boundaries. *Nanoscale* **2022**, *14*, 617−625.
(111) Shahriari, B.; Swersky, K.; Wang, Z.; Adams, R. P.; De Freitas, N. Taking the Human out of the Loop: A Review of Bayesian Optimization. *Proc. IEEE* **2016**, *104*, 148−175.
(112) Brochu, E.; Cora, V. M.; de Freitas, N. A Tutorial on Bayesian Optimization of Expensive Cost Functions, with Application to Active User Modeling and Hierarchical Reinforcement Learning. 2010, arXiv:1012.2599. arXiv.org e-Print archive. https://arxiv.org/abs/1012.2599.
(113) Mockus, J.; Tiesis, V.; Zilinskas, A. *The Application of Bayesian Methods for Seeking the Extremum*; Elsevier: Amsterdam, The Netherlands, 1978; Vol. 2, pp 117−129.
(114) Wang, Y.; Lv, J.; Zhu, L.; Ma, Y. Crystal Structure Prediction via Particle-Swarm Optimization. *Phys. Rev. B* **2010**, *82*, No. 094116.
(115) Wang, Y.; Lv, J.; Zhu, L.; Ma, Y. CALYPSO: A Method for Crystal Structure Prediction. *Comput. Phys. Commun.* **2012**, *183*, 2063−2070.
(116) Gao, B.; Gao, P. Y.; Lu, S. H.; Lv, J.; Wang, Y. C.; Ma, Y. M. Interface Structure Prediction via CALYPSO Method. *Sci. Bull.* **2019**, *64*, 301−309.
(117) Kresse, G.; Hafner, J. Ab Initio Molecular Dynamics for Liquid Metals. *Phys. Rev. B* **1993**, *47*, 558−561.
(118) Kresse, G.; Hafner, J. Ab Initio Molecular-Dynamics Simulation of the Liquid-Metal-Amorphous-Semiconductor Transition in Germanium. *Phys. Rev. B* **1994**, *49*, 14251−14269.
(119) Kresse, G.; Furthmüller, J. Efficiency of Ab-Initio Total Energy Calculations for Metals and Semiconductors Using a Plane-Wave Basis Set. *Comput. Mater. Sci.* **1996**, *6*, 15−50.
(120) Kresse, G.; Furthmüller, J. Efficient Iterative Schemes for Ab Initio Total-Energy Calculations Using a Plane-Wave Basis Set. *Phys. Rev. B* **1996**, *54*, 11169−11186.
(121) Shima, T.; Hu, S.; Luo, G.; Kang, X.; Luo, Y.; Hou, Z. Dinitrogen Cleavage and Hydrogenation by a Trinuclear Titanium Polyhydride Complex. *Science* **2013**, *340*, 1549−1552.
(122) Lazauskas, T.; Sokol, A. A.; Buckeridge, J.; Catlow, C. R. A.; Escher, S. G. E. T.; Farrow, M. R.; Mora-Fonz, D.; Blum, V. W.; Phaahla, T. M.; Chauke, H. R.; et al. Thermodynamically Accessible Titanium Clusters Ti_N, N = 2−32. *Phys. Chem. Chem. Phys.* **2018**, *20*, 13962−13973.
(123) Sakurai, M.; Watanabe, K.; Sumiyama, K.; Suzuki, K. Magic Numbers in Transition Metal (Fe, Ti, Zr, Nb, and Ta) Clusters Observed by Time-of-Flight Mass Spectrometry. *J. Chem. Phys.* **1999**, *111*, 235−238.
(124) Oosterom, G. E.; Reek, J. N. H.; Kamer, P. C. J.; van Leeuwen, P. Transition Metal Catalysis Using Functionalized Dendrimers. *Angew. Chem., Int. Ed.* **2001**, *40*, 1828−1849.
(125) Jiang, Y.-F.; Liu, J.-C.; Xu, C.-Q.; Li, J.; Xiao, H. Breaking the Scaling Relations for Efficient N_2-to-NH_3 Conversion by a Bowl Active Site Design: Insight from LaRuSi and Isostructural Electrides. *Chin. J. Catal.* **2022**, *43*, 2183−2192.
(126) Montemore, M. M.; Medlin, J. W. Scaling Relations between Adsorption Energies for Computational Screening and Design of Catalysts. *Catal. Sci. Technol.* **2014**, *4*, 3748−3761.
(127) Greeley, J. Theoretical Heterogeneous Catalysis: Scaling Relationships and Computational Catalyst Design. *Annu. Rev. Chem. Biomol. Eng.* **2016**, *7*, 605−635.
(128) Soon, A.; Sohnel, T.; Idriss, H. Plane-Wave Pseudopotential Density Functional Theory Periodic Slab Calculations of CO Adsorption on Cu_2O(111) Surface. *Surf. Sci.* **2005**, *579*, 131−140.
(129) Nolan, M.; Grigoleit, S.; Sayle, D. C.; Parker, S. C.; Watson, G. W. Density Functional Theory Studies of the Structure and Electronic Structure of Pure and Defective Low Index Surfaces of Ceria. *Surf. Sci.* **2005**, *576*, 217−229.
(130) Tsuji, Y.; Yoshida, M.; Kamachi, T.; Yoshizawa, K. Oxidative Addition of Methane and Reductive Elimination of Ethane and Hydrogen on Surfaces: From Pure Metals to Single Atom Alloys. *J. Am. Chem. Soc.* **2022**, *144*, 18650−18671.
(131) Gu, G.; Xiang, G.; Luo, J.; Tang, Z.; Zhang, X. The Structural, Electronic and Magnetic Properties of $Ga_{8-x}Mn_xAs_8$ Clusters. *J. Magn. Magn. Mater.* **2015**, *384*, 155−159.
(132) Diao, E.; Liu, X.; Tong, Q.; Liu, X. First Principles Data Driven Potentials for Prediction of Iron Carbide Clusters. 2022 DOI: 10.21203/rs.3.rs-1813606/v1.
(133) Tsuji, Y.; Hoffmann, R.; Miller, J. S. Revisiting $Ir(CO)_3Cl$. *Polyhedron* **2016**, *103*, 141−149.
(134) Perdew, J. P.; Burke, K.; Ernzerhof, M. Generalized Gradient Approximation Made Simple. *Phys. Rev. Lett.* **1996**, *77*, 3865−3868.
(135) Grimme, S. Accurate Description of van Der Waals Complexes by Density Functional Theory Including Empirical Corrections. *J. Comput. Chem.* **2004**, *25*, 1463−1473.
(136) Yang, T. T.; Tan, T. L.; Saidi, W. A. High Activity toward the Hydrogen Evolution Reaction on the Edges of MoS_2-Supported Platinum Nanoclusters Using Cluster Expansion and Electrochemical Modeling. *Chem. Mater.* **2020**, *32*, 1315−1321.

https://doi.org/10.1021/acsomega.3c03456
ACS Omega 2023, 8, 30335−30348

(137) Momma, K.; Izumi, F. VESTA 3 for Three-Dimensional Visualization of Crystal, Volumetric and Morphology Data. *J. Appl. Crystallogr.* **2011**, *44*, 1272−1276.

https://doi.org/10.1021/acsomega.3c03456
ACS Omega 2023, 8, 30335−30348